CHEMISTRY OF MATERIALS

pubs.acs.org/cm

Article

Composition-Dependent Optical Properties of Cu−Zn−In−Se Colloidal Nanocrystals Synthesized via Cation Exchange

Ankita Bora, Josephine Lox, René Hübner, Nelli Weiß, Houman Bahmani Jalali, Francesco di Stasio, Christine Steinbach, Nikolai Gaponik, and Vladimir Lesnyak*

Cite This: https://doi.org/10.1021/acs.chemmater.3c00538

Read Online

ACCESS | Metrics & More | Article Recommendations | Supporting Information

ABSTRACT: Copper chalcogenide-based nanocrystals (NCs) are a suitable replacement for toxic Cd/Pb chalcogenide-based NCs in a wide range of applications including photovoltaics, optoelectronics, and biological imaging. However, despite rigorous research, direct synthesis approaches of this class of compounds suffer from inhomogeneous size, shape, and composition of the NC ensembles, which is reflected in their broad photoluminescence (PL) bandwidths. A partial cation exchange (CE) strategy, wherein host cations in the initial binary copper chalcogenide are replaced by incoming cations to form ternary/quaternary multicomponent NCs, has been proven to be instrumental in achieving better size, shape, and composition control to this class of nanomaterials. Additionally, adopting synthetic strategies which help to eliminate inhomogeneities in the NC ensembles can lead to narrower PL bandwidths, as was shown by single-particle studies on I−III−VI_2-based semiconductor NCs. In this work, we formulate a two-step colloidal synthesis of Cu−Zn−In−Se (CZISe) NCs via a partial CE pathway. The first step is the synthesis of $Cu_{2-x}Se$ NCs, which serve as a template for the subsequent CE reaction. The second step is the incorporation of the In^{3+} and Zn^{2+} guest cations into the synthesized $Cu_{2-x}Se$ NCs via simultaneous injection of both metal precursors, which results in gradient-alloyed CZISe NCs with a Zn-rich surface. The as-synthesized NCs exhibit near-infrared (NIR) PL without an additional shell growth, which is typically required in most of the developed protocols. The photoluminescence quantum yield (PLQY) of these Cu chalcogenide-based NCs reaches 20%. These NCs also exhibit intriguingly narrow PL bands, which challenges the notion of broad PL bands being an inherent property of this class of NCs. Additionally, a variation in the feed ratios of the incoming cations, i.e., In/Zn, results in the variation of the composition of the synthesized NCs. Henceforth, the optical properties of these NCs could be tuned by a simple variation of the composition of the NCs achieved by varying the feed ratios of the incoming cations. Within a narrow size distribution, the PL maxima range from 980 to 1060 nm, depending on the composition of the NCs. Post-synthetic surface modification of the synthesized NCs enabled the replacement of the parent long-chain organic ligands with smaller species, which is essential for their prospective applications requiring efficient charge transport. With PL emission extended into the NIR, the synthesized NCs are suitable for an array of potential applications, most importantly in the area of solar energy harvesting and bioimaging. The large Stokes shift inherent to these materials, their absorption in the solar range, and their NIR PL within the biological window make them suitable candidates.

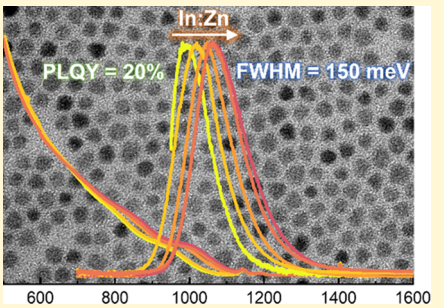

INTRODUCTION

Semiconductor nanocrystals (NCs) have been studied for their unique optical properties, which have established them as promising fluorophores due to their continuous absorption profiles, photostability, and tunable emission peaks.[1] Although a wide range of semiconductor NCs have been synthesized successfully, the ones studied most extensively are the II−VI and IV−VI semiconductors, such as CdSe and PbS, which have been exploited for optoelectronic and biomedical applications.[2,3] Despite the establishment of well-developed synthetic routes for these NCs and their appealing properties, the toxicity of cadmium and lead imposes problems for using them in some particular applications, especially those involving exposure to biological systems.[4] This calls for exploring alternatives to these materials, which can replicate the optical properties of the II−VI and IV−VI NCs and potentially replace them in the various applications.[5] This has led to a considerable effort to reveal alternative luminescent and photoactive metal chalcogenide compounds consisting of earth-abundant and less toxic elements. Amongst several options, I−III−VI_2 semiconductor quantum dots (QDs) have proven themselves as outstanding candidates to serve as an alternative for their more toxic counterparts.[6,7] Their benign composition makes them the best fit to be used in biological systems for bioimaging and drug delivery, which is one of the

Received: March 8, 2023
Revised: April 15, 2023

major applications of the semiconductor nanoparticles.[8] Most of the studies in the I−III−VI_2 family of materials have been done on $CuInS_2$ (CIS)-based compounds.[9] However, QDs based on $CuInSe_2$ (CISe) are of particular importance for light-harvesting owing to the small band gap of 1.04 eV of the bulk counterpart and the large excitonic Bohr radius of 10.1 nm compared to CIS, which has a comparatively larger band gap of 1.4 eV and a smaller Bohr radius of 4.1 nm.[10] These properties have been proven to be extremely instrumental in the development of photovoltaic cells employing CISe NCs, with power conversion efficiencies (PCEs) as high as 10%.[11] Even higher PCEs of 11.6 and 13.6% were reported for solar cells fabricated based on Cu−Zn−In−Se (CZISe) QDs by Du et. al. and Zhang et. al., respectively.[11,12] Efficient carrier multiplication should further improve the solar cell performance.[13,14] Moreover, CISe-based NCs are also explored as light harvesters in luminescent solar concentrators (LSCs) since the commonly observed large Stokes shift helps reducing the self-absorption losses, thereby increasing the photon conversion efficiency of the solar cells attached to these LSCs.[15−18]

Many strategies have been implemented for the synthesis of CISe NCs so far.[19] As a matter of fact, direct synthesis appears to be a reasonable option and has yielded small CISe NCs with PL tunable in the range of 600−1000 nm.[10,20−22] However, the multiple cations and anions existing in the reaction mixture in the case of direct synthesis each have different reactivities, and there exists a complex equilibrium that constrains a precise size, crystal structure, and composition control of the product NCs.[23] Taking into account the principle of hard and soft acids and bases,[24−26] one can understand that Cu^+, which is a soft acid, has a higher tendency to react with the soft base Se^{2-}, compared to the tendency of the hard acid In^{3+} reacting with Se species. In the direct synthesis of CISe NCs, this leads to the formation of $Cu_{2-x}Se$ first, resulting in the formation of additional byproducts other than the desired product. This lack of control over the reaction can be tackled by a cation exchange (CE) approach, which has been used as a convenient tool to synthesize a range of NCs, which otherwise would not have been possible via direct methods.[27−34] It also provides simultaneous control over the size, shape, composition, and crystalline structure of the material.[35] The process includes the synthesis of a binary compound, which serves as a template for the further incorporation of guest cations. Thus, while maintaining the anion framework, the guest cations are introduced into the crystal structure through a partial or complete exchange of the host cations to attain ternary and quaternary NCs. In this scenario, binary copper chalcogenides serve as suitable templates for CE reactions since Cu^+ is easily exchangeable with other cations.[27,28,36] The comparable ionic radii of the host Cu^+ cation and guest cations such as In^{3+} and Zn^{2+} in a given coordination number help in maintaining the structure and morphology of the NCs.[37,38] Additionally, the presence of a large number of copper vacancies in copper chalcogenides facilitate the exchange process by providing an additional route for the diffusion of the cations via the existing vacancies.[39]

Although extensive studies have been dedicated to developing synthetic strategies and plausible applications of copper chalcogenide-based nanomaterials, their light emission mechanism remains rather less understood. The most accepted PL mechanism is the radiative recombination of a photoexcited band-edge electron and a hole residing in an intragap state often associated with off-stoichiometric effects that have been shown to enhance the emission efficiency.[40−42] Studies on Cu-doped II−VI NCs have suggested that the intragap states reside in copper, and the similarities of these semiconductors to I−III−VI_2 semiconductors point in the direction that emission centers in these NCs are also Cu-related and the intragap recombination centers are native defects of these materials.[40,41] However, the oxidation state of Cu in these emissive centers is a matter of debates. While some studies show that the emissive center is Cu^+ because Cu exists in +1 oxidation state in CIS NCs, as indicated by X-ray photoelectron spectroscopy (XPS) studies,[43] some studies also emphasize the importance of the presence of paramagnetic Cu^{2+} defects for radiative exciton recombination.[40,44] Spectroelectrochemical studies by Fuhr et al. have shown both the Cu^+ and Cu^{2+} centers to be emissive with the dominance of Cu^{2+} defects in Cu-deficient QDs and Cu^+ in stoichiometric QDs.[45] Along with the emission mechanism, the underlying reasons for the peculiar PL properties of these NCs, in particular, the very long radiative lifetimes (100−500 ns), large Stokes shift (300−500 meV), and large PL broadening (>300 meV of full width at half-maximum (FWHM)), are also still under study.[46−48]

Long radiative lifetimes and large Stokes shift can be attributed to the intragap defects, which are native to this class of materials, thus making them inherent properties observed in all studied samples. The mechanism of PL broadening, however, does not have a cohesive explanation. Several studies have proposed different explanations for the origin of a broad PL.[40,43,49] Some suggested QDs' size polydispersity to be a plausible reason but that alone could not explain such broad PL, and the obscure mechanism behind it led to a prediction that it is also an intrinsic property of the material. However, this speculation has been challenged by recent single-particle spectroscopy studies.[50,51] Comparison of the PL linewidths of a single particle and a $CuInS_2$/ZnS QD ensemble by Zang et al. indicated that the broad PL is not an intrinsic property of these materials but a result of dot-to-dot variations in emission energy. It was observed that, for a particularly narrow size distribution, the PL bandwidth of a single particle was approximately 60 meV, compared to approximately 300 meV of the QD ensemble.[51] This suggests that, despite a narrow size distribution, the reason for broad PL can still be attributed to the ensemble heterogeneity in terms of its composition variation from particle to particle. Such variations in composition are most likely responsible for broad PL spectra, recently found also in thin CZIS nanoplatelets with uniform thickness and quite strong quantum confinement within the thickness dimension.[52] This sample heterogeneity results in a large number of Cu-related emission centers, which are positioned randomly. Such random positioning results in varying energy contributions from the electron−hole coupling to the total PL energy, exhibiting a broad PL spectrum. Thus, in principle, the PL linewidths of this class of materials can be reduced to the range of 100 meV. The challenge, however, is the development of synthetic strategies that will enable reducing the sample heterogeneity and thus the random positioning of emissive centers in the entire QD ensemble, resulting in narrower PL bands, which would be comparable to Cd and Pb chalcogenide-based NCs.

Here, we present a two-step synthesis of photoluminescent CZISe NCs using $Cu_{2-x}Se$ NCs as templates with subsequent simultaneous CE employing Zn^{2+} and In^{3+} as guest cations. In many cases, CISe QDs show no PL or low PLQY[9,53−55]

https://doi.org/10.1021/acs.chemmater.3c00538
Chem. Mater. XXXX, XXX, XXX−XXX

without an additional shell growth, which means that the NC surface is particularly prone to surface defects, thus increasing the number of centers for nonradiative recombination.[22] PLQY has been drastically increased by overcoating the NCs with wide band gap semiconductors such as ZnS or CdS.[20,21,56] In our case, the previously synthesized core CISe NCs did not show PL without shell growth, and only after the deposition of a ZnS shell, they exhibited a PLQY of less than 1%.[33] In this work, we were able to boost the PLQY up to 20% without growing the shell. While the generally observed broad PL remains a challenge in the case of I−III−VI_2 NCs, our synthetic strategy resulted in fairly narrow PL bands ranging from 150 to 190 meV. This supports the idea that the extremely broad PL on the order of 300 meV is not an intrinsic property of the material but rather a solvable issue. Along with the synthesis of CZISe NCs with enhanced PLQY and narrow PL spectra, we also varied the composition of the cations to draw a relation between the composition of the as-synthesized NCs and their optical properties. Within a narrow size distribution, the PL was tunable in the range from 980 to 1060 nm with a simple variation in the NC composition. In addition, we present three possible routes of ligand exchange, wherein parent long-chain organic ligands on the surface of the NCs are exchanged with shorter new ligands to make them compatible for prospective applications of solar energy harvesting. Its potential use in the fabrication of solution-based solar cells is still under study.

EXPERIMENTAL SECTION

Materials. Copper(II) acetylacetonate ($Cu(acac)_2$, 97%), indium(III) acetate ($In(OAc)_3$, 99.99%), Se powder (99.99%), zinc(II) acetate ($Zn(OAc)_2$, 99.99%), ammonium sulfide solution ($(NH_4)_2S$, 20 wt % in H_2O), triethyloxonium tetrafluoroborate (Et_3OBF_4, ≥97%), zinc bromide ($ZnBr_2$, 99.99%), octadecene (ODE, technical grade, 90%), octylamine (OctAm, 99%), oleylamine (OlAm, 70%), toluene (≥99.7%), tetrachloroethylene (TCE, 99%), dodecanethiol (DDT, 99%), and chloroform (≥99%) were purchased from Sigma-Aldrich. Tri-*n*-octylphosphine (TOP, 97%), hexane (97%), and methanol (99.9%) were purchased from VWR. *N*-Methylformamide (MFA, 99%) and extra-dry acetonitrile (99.9%) were purchased from Acros Organics. 1-Butylamine (99%) was purchased form Alfa Aesar. Dimethylformamide (DMF, analytical reagent grade) was purchased from Fischer Chemicals. All chemicals were used without any further purification.

Synthesis of $Cu_{2-x}Se$ NCs. The parent $Cu_{2-x}Se$ NCs were synthesized using a previously published protocol.[33] First, a Se-precursor solution was prepared by dissolving 790 mg (10 mmol) of Se powder in 5 mL of DDT and 5 mL of OlAm under vacuum at 50 °C for 1 h. After the complete transformation of Se into a brown alkylammonium selenide, the precursor solution was cooled down and stored in a nitrogen-filled glove box. For the synthesis of $Cu_{2-x}Se$ NCs, 0.5254 g (2 mmol) of $Cu(acac)_2$ was dissolved in 18 mL of OlAm and 9 mL of DDT upon vigorous stirring under vacuum at 60 °C for 1 h to produce a translucent white dispersion. Thereafter, the flask was filled with N_2 and the temperature was raised to 140 °C. With the increase in temperature, the solution became transparent and yellowish-green in color. Once the required temperature was attained, 1.32 mL (1.32 mmol) of the Se-precursor were injected. In 30 s after the injection, the heating mantle was removed swiftly and the reaction mixture was allowed to cool down to room temperature. The crude reaction mixture of $Cu_{2-x}Se$ NCs without any additional modification was used as parent NCs for the exchange with In^{3+} and Zn^{2+} cations (see the next section). An aliquot of 0.2 mL of the reaction mixture was taken out and precipitated by adding methanol, followed by centrifugation at a speed of 5100 rpm for 5 min and finally redispersed in toluene and stored for further characterization. For the synthesis of larger CZISe NCs for elemental mapping, the size of the parent $Cu_{2-x}Se$ NCs was increased by an increase in reaction temperature from 140 to 200 °C. The reaction time was also increased to 4 min along with a decrease of the Cu/Se ratio from 1.5:1 to 1:1.

Synthesis of CZISe NCs. Using the synthesized $Cu_{2-x}Se$ NCs as templates, a mixture of the In- and Zn-precursors was injected for a combined CE reaction to occur between the host Cu^+ cations and the guest In^{3+} and Zn^{2+} cations. The In-precursor was prepared by dissolving 1.0213 g (3.5 mmol) of $In(OAc)_3$ in 5.25 mL of OctAm, 5.25 mL of OlAm, and 31.5 mL of ODE in a 100 mL flask upon stirring under vacuum at 60 °C. Then, the flask was filled with N_2, and thereafter the temperature was raised to 150 °C to prepare a clear solution. Subsequently, the heating mantle was removed, and the solution was allowed to cool down to room temperature. Thereafter, 10.5 mL of TOP was added, and the precursor was stored in the glove box. The Zn-precursor was prepared by dissolving 1.83 g (10 mmol) of $Zn(OAc)_2$ in 5 mL of OlAm and 5 mL of OctAm under vacuum at 40 °C for 1 h. Thereafter, N_2 was passed, and the temperature was increased to 100 °C for a clear solution to form. Subsequently, the temperature was decreased by removal of the heating mantle, and upon reaching room temperature, the precursor solution was transferred to the glove box. For the exchange, the required amounts of the In- and Zn-precursors were mixed inside the glove box and then transferred to a flask purged with N_2. The temperature was raised to 220 °C, and 5 mL (0.3531 mmol) of the crude reaction mixture containing $Cu_{2-x}Se$ NCs were swiftly injected. The temperature was maintained for 20 min along with continuous stirring of the reaction mixture. Thereafter, the heating mantle was removed, and the reaction mixture was allowed to cool down to room temperature and was precipitated with methanol, followed by centrifugation at a speed of 5100 rpm for 5 min. The particles were purified two times by redissolving in toluene and precipitating with methanol. To study the composition dependence of the optical properties, various ratios of Cu/Zn/In were used: 1:1:1, 1:1:2, 1:1:0.5, 1:2:1, and 1:0.5:1.

Transmission Electron Microscopy (TEM). Sample preparation for a conventional TEM analysis included additional purification of the NCs via reprecipitation and preparation of a diluted NC solution in toluene. This solution was drop-cast onto a carbon-coated copper grid with subsequent evaporation of the solvent. Conventional TEM imaging was carried out on a JEOL JEM-1400 microscope equipped with a thermionic gun (W filament) working at an accelerating voltage of 120 kV. High-angle annular dark-field scanning TEM (HAADF-STEM) imaging and spectrum imaging analyses based on energy-dispersive X-ray spectroscopy (EDXS) were performed on a Talos F200X microscope operated at 200 kV and equipped with an X-FEG electron source and a Super-X EDX detector system (FEI). Prior to STEM analysis, the specimen mounted in a high-visibility low-background holder was placed for 2 s into a Model 1020 Plasma Cleaner (Fischione) to remove potential contamination. For the STEM-based analyses, the NC solution in toluene was drop-cast onto carbon-coated Ni grids to avoid Cu fluorescence radiation.

Powder X-ray Diffraction (XRD) Analysis. The samples were prepared by drop-casting concentrated NC dispersions onto a zero-background silicon wafer. XRD patterns were recorded on a Bruker D2 Phaser using an X-ray tube with a Cu anode operated at 30 kV and 10 mA. WinXPow software with references from the Inorganic Crystal Structure Database was used for analysis.

UV−Vis−NIR Absorption Spectroscopy. Samples were prepared by diluting dispersions of the NCs with TCE. The absorption spectra were recorded on a Cary 5000 UV−vis−NIR spectrophotometer (Varian) using 1 cm path quartz cuvettes.

Photoluminescence Measurements. Steady-state PL spectra were recorded by dispersing the NCs in TCE, while PLQY and PL lifetime measurements were carried out using NC dispersions in toluene. The PL spectra were recorded on a FluoroLog-3 spectrofluorometer (Horiba Jobin Yvon Inc.) using an excitation wavelength of 450 nm. Absolute PLQY measurements were performed on an Edinburgh Instruments spectrofluorometer FLS900 (equipped with a Xe lamp, PMT-1700 and calibrated

https://doi.org/10.1021/acs.chemmater.3c00538
Chem. Mater. XXXX, XXX, XXX−XXX

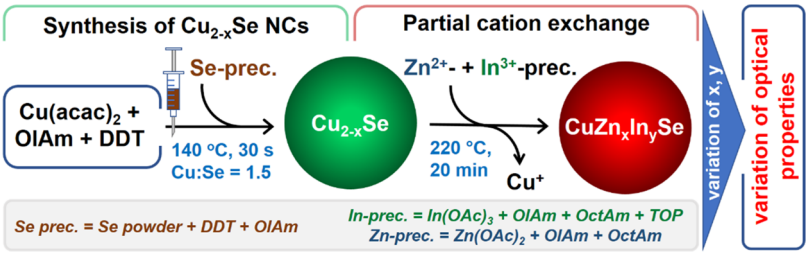

Figure 1. Scheme depicting the synthesis of $Cu_{2-x}Se$ NCs with subsequent partial CE to CZISe NCs, followed by the study of the composition dependence of their optical properties.

integrating sphere). All samples were excited at 700 nm, and their concentration was adjusted to an optical density of 0.15 at the excitation wavelength. The PLQY values were calculated by Flouracle software. The time-resolved PL traces were collected using an Edinburgh Instruments EPL-510 pulsed laser diode for excitation (λ = 508.2 nm, pulse width = 177.0 ps) and a time-correlated single photon counting (TCSPC) card.

Elemental Analysis. The samples for inductively coupled plasma optical emission spectroscopy (ICP-OES) were prepared by decomposing the particles in aqua regia with subsequent dilution with Milli-Q water. The analysis was done on a Thermo Fisher iCap7000 instrument to quantify the copper, indium, and zinc contents in the synthesized NCs.

Fourier Transform Infrared (FTIR) Spectroscopy. Attenuated total reflectance (ATR) FTIR spectra were recorded on a Thermo Scientific Nicolet iS5 FTIR spectrometer. Concentrated solutions of NCs in an appropriate solvent were directly drop-cast on the ATR crystal, and the solvent was left to evaporate.

RESULTS AND DISCUSSION

The first step of the CZISe NC synthesis involves the preparation of small, approximately 5 nm-sized $Cu_{2-x}Se$ NCs using a hot-injection approach (see Figure 1). The second step is the simultaneous CE of Cu^+-to-In^{3+} and -Zn^{2+}. In this process, the ratio of the guest cations was varied to study the influence of the composition on the optical properties. This variation in composition of the guest cations alone enabled to tune the position of the PL maxima in the NIR region.

Synthesis of $Cu_{2-x}Se$ NCs. The synthesis of the template $Cu_{2-x}Se$ NCs was carried out using a modified version of a previously published protocol.[33,39,57,58] Aiming at the growth of small, approximately 5 nm-sized NCs, we used the initial Cu/Se ratio of 1.5 and 30 s reaction time, as reported earlier, wherein a relatively low reaction temperature of 140 °C offered a better control over the NC size.[33] A short reaction time and a relatively low temperature are instrumental in the synthesis of small $Cu_{2-x}Se$ NCs. Furthermore, a Cu/Se ratio of 1.5 results in forming nonstoichiometric $Cu_{2-x}Se$ NCs, which then serve as a suitable template for the subsequent partial CE reaction. TEM imaging of these NCs revealed fairly monodisperse spherical particles (see Figure 3a) with an average size of 4.4 ± 0.1 nm (their size distribution histogram is displayed in Figure S1a). XRD analysis confirmed their cubic berzelianite crystal structure (ICSD C6-680, Figure 2).

Synthesis of CZISe NCs with Varying Composition. In the subsequent step, a simultaneous CE of Cu^+-to-In^{3+} and -Zn^{2+} was carried out. In this approach, the In-precursor prepared by dissolving $In(OAc)_3$ in OlAm, OctAm, ODE, and TOP was mixed with the Zn-precursor prepared by dissolving $Zn(OAc)_2$ in OlAm and OctAm, and the mixture was heated to 220 °C (see Figure 1). As soon as the desired temperature was attained, the $Cu_{2-x}Se$ NCs were injected swiftly, and the

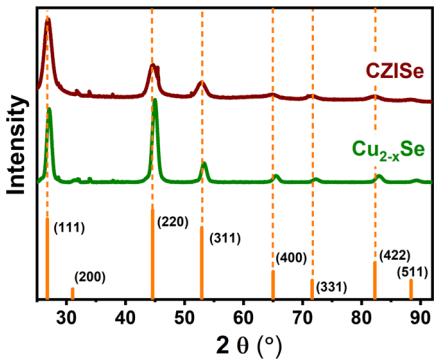

Figure 2. XRD patterns of template $Cu_{2-x}Se$ and exchanged CZISe NCs after simultaneous partial CE. The experimental XRD patterns are compared to the powder diffraction file database entry of cubic berzelianite (ICSD C6-680).

temperature was maintained for 20 min. Upon addition of the guest cations, the dark green color of the template NCs changes to dark brown, indicating the successful CE reaction. Two factors aid this exchange process. First, TOP present in the In-precursor solution being a soft base binds preferentially with Cu^+ (a soft acid), leading to its efficient extraction from the NC lattice, thus facilitating the incorporation of In^{3+} and Zn^{2+}.[24,35,59,60] Second, the presence of Cu vacancies boosts the CE by providing additional diffusion pathways for the incoming and outgoing cations.[39,61] A relatively high temperature of 220 °C was used because, at higher temperatures, the reactivity of Zn^{2+} increases, thus enabling the diffusion of Zn^{2+} cations into the core of the NCs instead of replacing Cu^+ just on the surface. It was observed by Akkerman et al. that, at elevated temperature and with simultaneous addition of guest cations, homogeneously alloyed CZIS NCs could be formed, while upon sequential addition at lower temperatures, gradient-alloyed CZIS NCs with a ZnS-rich surface were obtained.[38]

TEM images of the NCs synthesized reveal their quasi spherical shape and a narrow size distribution (in Figure 3b,c CZISe NCs with two different compositions, Zn-poor and Zn-rich, are shown; CZISe NCs of other compositions are shown in Figure S2, the histograms representing the NC size distribution are shown in Figure S1b−f). Comparing the TEM image of the template $Cu_{2-x}Se$ NCs presented in Figure 3a and the TEM images of CZISe NCs, we can conclude that the morphology undergoes no change owing to the fact that the anion framework is maintained during the CE reaction.[33] The evaluated NC sizes summarized in Table 1 indicate a slight increase in size after the CE reaction, possibly due to their simultaneous growth during the exchange. We point out that the sizes of all different compositions depicted in Table 1

https://doi.org/10.1021/acs.chemmater.3c00538
Chem. Mater. XXXX, XXX, XXX−XXX

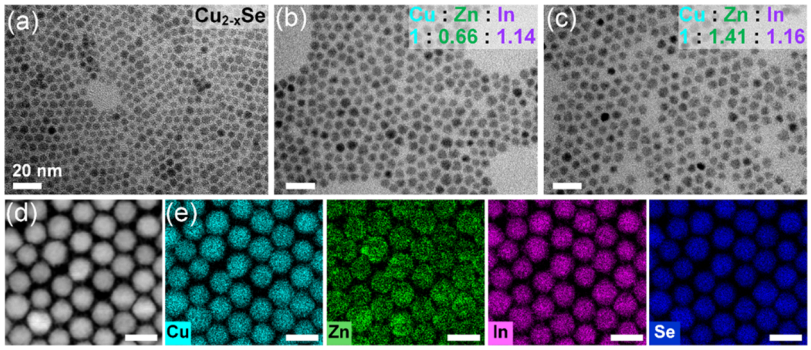

Figure 3. TEM images of template $Cu_{2-x}Se$ NCs (a) and exchanged CZISe NCs with the final Cu/Zn/In ratio of 1:0.66:1.14 (b) and 1:1.41:1.16 (c). HAADF-STEM image (d) and corresponding EDXS-based elemental distribution maps (e) of large CZISe NCs with a Cu/Zn/In ratio of 1:1:1. In all images, the indicated scale bar is 20 nm.

Table 1. Initial Feed Ratios, Final Composition, In/Zn Ratio, and Average Sizes of the CZISe NCs

initial Cu/Zn/In	final Cu/Zn/In	In/Zn	Cu/(In + Zn)	size (nm)
1:1:1	1:0.91:1.13	1.24	0.48	5.02 ± 0.8
1:1:2	1:0.84:1.36	1.60	0.45	5.2 ± 0.7
1:1:0.5	1:1.18:0.96	0.81	0.46	5.0 ± 0.7
1:2:1	1:1.4:1.16	0.82	0.38	5.0 ± 0.7
1:0.5:1	1:0.66:1.14	1.72	0.55	5.2 ± 0.6

are similar, and therefore, the size effect on the resulting properties of the NCs can be neglected. To gather more insight into the morphology and elemental distribution of the NCs, HAADF-STEM imaging and spectrum imaging analyses based on EDXS were carried out on larger, 12 nm-sized CZISe NCs. The HAADF-STEM image in Figure 3d shows that these NCs are spherical in shape, and the corresponding EDXS-based elemental maps shown in Figure 3e indicate rather homogeneous distributions of Cu and In, which also correspond well with the distribution of Se, while Zn appears to be distributed more inhomogeneously with a larger concentration in the outer layer. Thus, starting with non-stoichiometric $Cu_{2-x}Se$ NCs, the strategy of simultaneous CE to In^{3+} and Zn^{2+} results in the growth of gradient alloy-like NCs with In^{3+} replacing Cu^{+} in the whole NC as well as Zn^{2+} more preferentially on the surface, contrary to homogeneously alloyed CZIS NCs obtained from Cu_2S NCs via simultaneous CE by Akkerman et al.[38]

As seen from the XRD patterns in Figure 2, the positions and the intensity of the peaks indicate the preservation of the crystal structure, which is expected from a CE approach. It is a commonly observed effect of CE reactions, wherein the anion framework remains intact while the exchange of host cations by guest cations takes place. Given that the ionic radii of Cu^{+}, In^{3+}, and Zn^{2+} are comparable in both the tetrahedral and octahedral coordinations, there is most likely efficient exchange of the cations only while maintaining the integrity of the anion framework.[37,38] This simple strategy is used as a tool to synthesize CIS NCs with metastable crystal structures rather than the thermodyamically stable counterparts. In general, CIS(Se) crystallizes in the cubic or tetragonal phase (derived by the distortion of the zinc blende phase), depending on the reaction temperature and composition.[62] However, metastable hexagonal CIS has been formed using a CE pathway by Akkerman et al., wherein they started from hexagonal $Cu_{2-x}S$ NCs in which a subsequent addition of In^{3+} and Zn^{2+} cations did not lead to restructuring, thus resulting in metastable hexagonal CIS and CZIS NCs.[38] Similarly, a metastable hexagonal crystal structure of CIS NCs was observed by Pan et al.[63] Consequently, in our case, also the initial crystal structure of the template NCs was preserved during the exchange. The positions of the diffraction peaks shift slightly to lower Bragg angles compared to the position of the initial $Cu_{2-x}Se$ NCs, which indicates filling of the copper vacancies by the incoming guest cations.[33]

The composition of the final NCs was controlled by a simple variation in the feed ratio of the guest cations. The initial feed ratios, the final composition derived from ICP-OES, and the corresponding sizes of the different CZISe NCs are summarized in Table 1. The ICP-OES results show that the Cu/Zn/In feed ratio of 1:1:1 results in a Cu/Zn/In ratio of 1:0.91:1.13 with In replacing 37.4% of the Cu ions and Zn replacing 29% of the Cu ions. This implies that the Cu^{+}-to-In^{3+} CE is more feasible than the Cu^{+}-to-Zn^{2+} one. However, there is also the possibility of a simultaneous Zn^{2+}-to-In^{3+} CE leading to a larger amount of In in the NCs. It was observed previously that, even by using a large excess of a Zn-precursor, the Zn content could not be increased above a certain limit, which also suggests that Zn^{2+} can only partially replace Cu^{+} and is less efficient than the Cu^{+}-to-In^{3+} CE.[38] In our case, first, the In amount was increased with a Cu/Zn/In feed ratio of 1:1:2 resulting in the final ratio of 1:0.84:1.36. Thus, even by doubling the In-precursor content, there is no complete Cu^{+}-to-In^{3+} CE observed with In^{3+} replacing only 42.6% of Cu, while Zn^{2+} replaces 26.4% of the Cu^{+} cations. Thus, even though the Cu^{+}-to-In^{3+} CE is more feasible, a competition between both exchanges makes it difficult to precisely control the reaction. Consequently, a decrease in the In-precursor concentration leads to a decrease in the amount of In vs Zn. Thereafter, the Zn content was also varied by using a Cu/Zn/In feed ratio of 1:2:1, resulting in the final ratio of 1:1.4:1.16. This obviously led to increasing the efficiency of the Cu^{+}-to-Zn^{2+} CE resulting in Zn replacing 39.5% of Cu^{+} and In replacing 32% of Cu^{+}. A decrease in the Zn amount in the Cu/Zn/In feed ratio of 1:0.5:1 subsequently decreased the Zn content in the NCs, resulting in a final Cu/Zn/In ratio of 1:0.66:1.14. Thus, it can be concluded that, while there is a higher feasibilty of the Cu^{+}-to-In^{3+} CE, there exists a competition between both exchanges which cannot be precisely controlled, resulting in varying compositions of the NCs.

It is also noteworthy that the entire reaction takes place without an intermediate NC purification step, thus leaving the possibility of unreacted Cu^{+} from the first step interfering in

https://doi.org/10.1021/acs.chemmater.3c00538
Chem. Mater. XXXX, XXX, XXX−XXX

the CE step, hence adding to the difficulty of precise composition control of the resulting CZISe NCs. Additional purification might lead to the stripping of the parent ligands inducing the instability of the NC colloids and deterioration of the optical properties, and therefore, such purification was avoided. When the In/Zn feed ratio is plotted against the final In/Zn ratio, we observe an increasing trend of the In/Zn ratio, as shown in Figure 4. Additionally, as seen in the graph, the final ratio of the host cations to the combined ratio of the guest cations, i.e., Cu/(In + Zn), does not show significant changes depending on the In/Zn feed ratio, thus indicating that the ratio between the host and the guest cations is roughly similar for all compositions independent of the varying ratio between the guest cations.

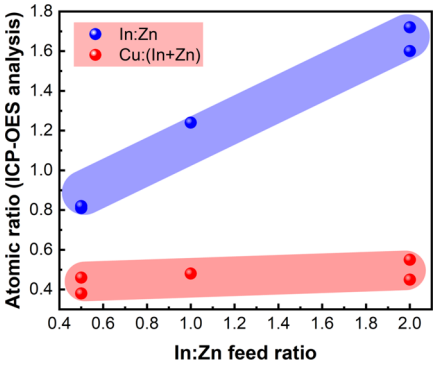

Figure 4. In/Zn and Cu/(In + Zn) atomic ratios obtained from ICP-OES analysis plotted vs the In/Zn feed ratio.

Optical Properties of CZISe NCs with Varying Composition. The as-synthesized NCs were characterized by absorption and PL spectroscopy. The template $Cu_{2-x}Se$ NCs exhibit a localized surface plasmon resonance (LSPR) peaking at approximately 1100 nm, as shown in Figure S3, which is commonly observed in this material and attributed to the collective oscillation of free holes.[33,39,57,58] These free holes in the valence band originate from a large number of copper vacancies present in the crystal structure.[64,65] The presence of the vacancies is instrumental for CE with vacancy diffusion driving the exchange along with other factors. As indicated by the absorption spectra in Figure 5a, a successful CE reaction is accompanied by the LSPR dampening, a profound indication of the filling of copper vacancies.[39,57] Analysis of the absorption spectra reveals the presence of a broad shoulder at around 900−1000 nm, marking the first electronic transition, which is generally observed in small CISe NCs.[66,67] Such shoulder in the absorption spectra of CZISe NCs was also reported by Du et al., wherein their 4 nm-sized NCs exhibited a shoulder at around 860−980 nm depending on the synthesis temperature.[11] Featureless absorption generally observed in I−III−VI_2-based NCs is attributed to the inhomogeneous composition of the NC ensemble.[33,68] Thus, the presence of excitonic features in the NCs highlights their homogeneous composition, as well as uniform size and shape. For higher In/Zn ratios, one can distinguish an additional broad shoulder at around 850 nm, which can be attributed to the second electronic transition, a phenomenon practically not observed in I−III−VI_2-based NCs. As far as the composition dependence of the onset of absorption is concerned, we observe a blue shift with the increase in Zn content: the NCs with an In/Zn ratio of 0.81 and 0.82 exhibit the most blue-shifted onset at approximately 1050 nm. For higher In/Zn ratios, i.e., a lesser amount of Zn, the absorption onset is slightly red-shifted. It is a general observation, wherein a larger Zn content leads to widening of the band gap and a blue shift of the absorption onset. For example, Zhang et al. observed that the absorption onset of CZISe NCs exhibited a blue shift with increased Zn amount.[12] A similar widening of the band gap reflected in the blue shift of the absorption band was observed by De Trizio et al. by incorporation of Zn^{2+} via partial CE into presynthesized CIS NCs.[69]

Figure 5b depicts the PL spectra of the various compositions of CZISe NCs. The PL bands are narrower compared to spectra generally reported for I−III−VI_2-based NCs. Most PL bandwidths reported are in the range of about 300 meV, and it is believed to be an intrinsic property of the material.[50,51] Contrary to this, single-particle studies pointed toward the underlying reason of the broad PL to be simply the sample heterogeneity. In particular, Zang et al. suggested that the PL bandwidths of CIS NCs can be lowered to approximately 100 meV, the only challenge being the development of synthetic strategies for preparing NCs showing such narrow spectra.[51] Hinterding et al. also showed that the single-particle PL spectra were approximately two times narrower than those of the ensemble of the CIS core and CIS/CdS core/shell NCs.[70] This line broadening was assigned to the sample inhomogeneity originating from polydispersity in size, shape, and composition. In our case, the ensemble PL bandwidths could be narrowed to the range of 150−190 meV, which we attribute to the structural homogeneity, also supported by the absence of multiple features in the PL spectra.[16,46]

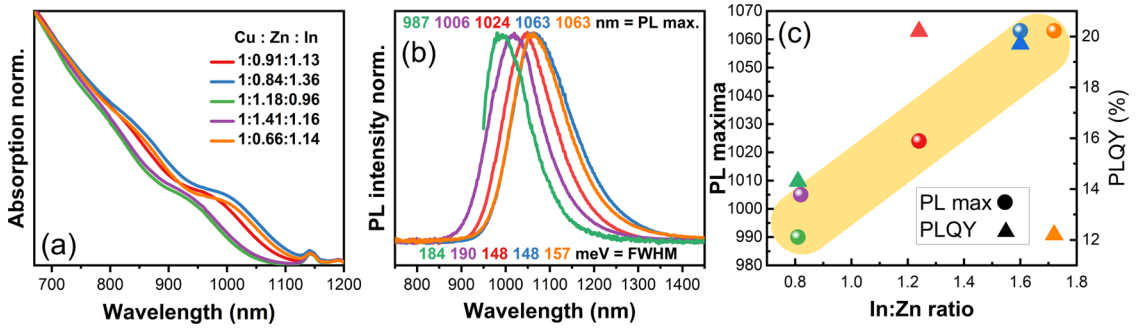

Figure 5. Absorption (a) and PL (b) spectra of CZISe NCs with Cu/Zn/In atomic ratios of 1:0.91:1.13, 1:0.84:1.36, 1:1.18:0.96, 1:1.4:1.16, and 1:0.66:1.14. (The small peak in panel (a) at approximately 1140 nm is an absorption feature of the solvent.) Trend of PL maxima and PLQY values plotted vs the In/Zn atomic ratio (c).

https://doi.org/10.1021/acs.chemmater.3c00538
Chem. Mater. XXXX, XXX, XXX−XXX

PLQY values of these NIR-emitting CZISe NCs range from 12.2% (In/Zn ratio of 1.72) to 20.2% (In/Zn ratio of 1.24), as plotted in Figure 5c. CZISe NCs with an In/Zn ratio of 0.81 exhibited a PLQY of 14.3% and those with an In/Zn ratio of 1.60 showed a PLQY of 19.7%. Apparently, the PLQY values did not follow a particular trend with varying In/Zn ratio, but the stoichiometric feed ratio of Cu/In/Zn resulted in the highest PLQY. The PLQY of ternary/quaternary I−III−VI_2-based NCs can be increased considerably with the growth of a shell. For instance, a PLQY of as high as 60% has been reported for CISe/ZnS core/shell NCs.[9] Akkerman et al. also observed an enhanced PL in the case of sequential CE on $Cu_{2-x}S$ NCs resulting in a ZnS-rich surface and finally leading to the formation of a gradient-type CZIS/ZnS structure rather than a homogeneously alloyed one.[38] However, they found no PL in the case of simultaneous CE, unlike in our case. PLQY reported previously by us for CZISe/ZnS NCs was <1%;[33] thus, we achieved a manyfold increase with this synthetic strategy. The enhancement of PL efficiency can directly be related to the incorporation of Zn^{2+}, as was shown by De Trizio et al. on the example of $Cu_{1-x}InS_2$ NCs, wherein partial CE with Zn resulted in record PLQY values of 80%.[69] Zn^{2+} cations tend to fill defects on the NC surface, thus eliminating the channels for nonradiative recombination. Time-resolved PL traces of our CZISe NCs are presented in Figure S4. The average PL lifetime values are 120, 154, 223, and 115 ns for CZISe NCs with Cu/Zn/In ratios of 1:0.91:1.13, 1:0.84:1.36, 1:1.41:1.16, and 1:0.66:1.14, respectively. In general, copper chalcogenide-based NCs exhibit very long PL lifetimes on the range of hundreds of nanoseconds.[43,71] Long radiative lifetimes of these NCs originate from the complex recombination mechanism proceeding through intragap states. In addition, PL decay curves of Cu chalcogenide-based NCs usually cannot be fitted with single exponential functions reflecting multiple recombination pathways existing in the NC ensemble.[41,49,71]

Previous studies have shown that the incorporation of Zn triggers a blue shift of the PL maxima caused by widening of the band gap.[69,72] Consequently, a larger Zn^{2+} content will result in a more pronounced blue shift of the PL maxima. For example, Liu et al. tuned the PL maxima of 2.6 nm-sized CZISe NCs synthesized via an aqueous approach in the range of 600−800 nm with larger Zn contents leading to a blue shift.[72] However, in our case, a simultaneous CE is carried out, and the final position of the PL maxima would undoubtedly depend on both the In and Zn content; therefore, it was reasonable to plot the PL maxima vs the In/Zn ratio to deduce a possible composition dependence (see Figure 5c). The ratio of Cu to the sum of the guest cations was practically constant for all samples, with the compositions of Cu/Zn/In = 1:0.91:13, 1:0.84:1.36, 1:1.18:0.96, 1:1.41:1.16, and 1:0.66:1.14, yielding Cu/(In + Zn) of 0.48, 0.45, 0.46, 0.4, and 0.50, respectively. This means that the variation of optical properties can simply be attributed to the relative ratio of incoming cations. Regarding the composition dependence of the PL, we see a blue shift with the increase in the Zn content vs In. For the In/Zn ratios of 0.81 and 0.82, the most blue-shifted emission was observed at 987 and 1006 nm, respectively. With further increase in In content, leading to a In/Zn ratio of 1.2, the PL maxima were red-shifted to 1024 nm. Consequently, even higher In/Zn ratios of 1.6 and 1.7 led to the most red-shifted emission at 1063 nm. Thus, we could tune the PL maxima from approximately 980 to 1060 nm by a simple variation of the ratio of incoming cations in the same size range.

Ligand Exchange. The as-synthesized CZISe NCs were capped with OlAm and DDT, long-chain organic ligands, revealed by an intensive characteristic C−H band in the FTIR spectrum depicted in Figure S5. While the presence of ligands on the surface of the NCs is necessary for their growth and stability, the long-chain ligands also act as barriers for charge transfer and reduce electronic coupling between adjacent NCs.[32,73,74] Therefore, the long ligands on the surface of the NC core are in fact detrimental for the use of these NCs in various optoelectronic applications where efficient charge transport is required, e.g., in solar cells[11,32,67] and field effect transistors.[32,75] To make CZISe NCs compatible for prospective applications, the parent ligands have to be exchanged or removed. Such solution-based ligand exchange also simplifies the device fabrication, wherein film deposition via layer-by-layer ligand exchange can be avoided.[32]

In a first attempt, the parent organic ligands were exchanged with inorganic sulfide ligands (experimental details are provided in the Supporting Information). For this, a biphasic mixture of the NCs in hexane and ammonium sulfide in MFA was kept under stirring overnight, resulting in the NC transfer to the polar MFA phase, as shown in Figure 6a. The ligand

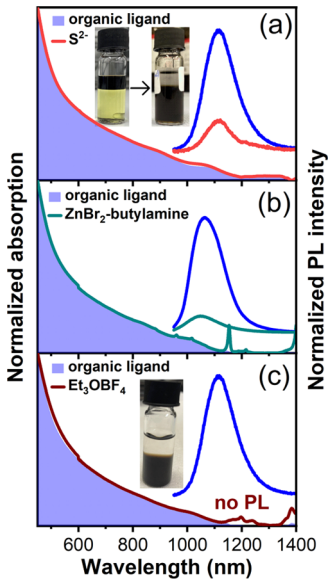

Figure 6. Absorption and PL spectra of CZISe NCs before and after ligand exchange with S^{2-} (a), $ZnBr_2$-butylamine (b), and Et_3OBF_4 (c). The inset in panel (a) shows the transfer of the NCs from hexane to the MFA phase, and the inset in panel (c) shows the NCs after transfer into the acetonitrile phase.

exchange was further confirmed by the significant reduction of the $-CH_2-$ band, which is quite intense in the FTIR spectrum of as-synthesized NCs (see Figure S5). Concentrated dispersions of CZISe NCs with the new ligands could also be prepared in DMF, which can then be directly used for device fabrication. The optical properties, i.e., absorption and position of the PL maximum, remained unchanged after the exchange, as shown in Figure 6a, while PL intensity dropped due to the introduction of surface defects.

The second strategy was to exchange the parent organic ligands with $ZnBr_2$ and butylamine. $ZnBr_2$ solution in methanol was added to the NC dispersion in toluene until it

https://doi.org/10.1021/acs.chemmater.3c00538
Chem. Mater. XXXX, XXX, XXX−XXX

turned turbid, indicating the promotion of the ligand exchange. This turbid solution was reversed to a clear solution by adding butylamine. The ligand exchange was reflected in a decreased intensity of the $-CH_2-$ band, as shown in the FTIR spectrum in Figure S5. Concentrated dispersions of $ZnBr_2$–butylamine-capped CZISe NCs could be prepared in chloroform, which might be useful for the fabrication of thin films via solution-based processing. The last strategy tested was adopted from Rosen et al., which led to the stripping off of the parent ligands,[32,76] as proven by the absence of the $-CH_2-$ band in the FTIR spectrum (Figure S5). The NCs capped with BF_4^- could be dispersed in DMF to form concentrated colloids. The absorption spectrum after the exchange remained the same, as depicted in Figure 6c, while emission disappeared due to the formation of surface defects, which can serve as centers for nonradiative recombination. Thus, the surface modification of these NCs was possible despite the presence of strongly bound thiol ligands, and concentrated batches of CZISe NCs could be prepared. These surface-modified NCs could further be used for prospective applications, particularly in solar energy harvesting due to the suitability of the band gap of the material and its nontoxic nature.[67] While solar cells fabricated employing CZISe NCs with a PCE of 13.6% have been reported,[12] further efforts to increase the PCE of the devices need to be undertaken.

CONCLUSIONS

We developed a simultaneous CE approach to the synthesis of CZISe NCs with considerably good optical properties. In particular, the FWHM of their NIR PL was reduced to 150–190 meV and the PLQY was increased to 20%. These properties are quite rarely observed for Cu chalcogenide-based ternary/quaternary NCs without an additional shell growth. Furthermore, we could also draw a relation between the optical properties and the composition of the CZISe NCs. In agreement with the generally observed trend of an increasing blue shift with the increase in the Zn content, we could introduce a blue shift by increasing the Zn content. The increase in In content led to an opposite trend, i.e., a PL red shift. Thus, upon controlling the In/Zn ratio, we were able to tune the PL in the range of approximately 980–1060 nm. The organic ligands on the surface of the as-synthesized NCs could be exchanged with short-chain ligands, thus decreasing the distance between adjacent NCs in the solids, which should significantly improve their electronic coupling. This possibility keeps the door for prospective applications of these NCs in solar energy harvesting open.

ASSOCIATED CONTENT

Supporting Information

The Supporting Information is available free of charge at https://pubs.acs.org/doi/10.1021/acs.chemmater.3c00538.

TEM image of $Cu_{2-x}Se$ NCs and size distribution histograms of $Cu_{2-x}Se$ and CZISe NCs; absorption spectrum of $Cu_{2-x}Se$ NCs; PL lifetime traces of CZISe NCs with different composition, and FTIR spectra of CZISe NCs with different ligands (PDF)

AUTHOR INFORMATION

Corresponding Author

Vladimir Lesnyak – *Physical Chemistry, TU Dresden, 01069 Dresden, Germany;* orcid.org/0000-0002-2480-8755; Email: vladimir.lesnyak1@tu-dresden.de

Authors

Ankita Bora – *Physical Chemistry, TU Dresden, 01069 Dresden, Germany*

Josephine Lox – *Physical Chemistry, TU Dresden, 01069 Dresden, Germany*

René Hübner – *Institute of Ion Beam Physics and Materials Research, Helmholtz-Zentrum Dresden-Rossendorf e.V., 01328 Dresden, Germany;* orcid.org/0000-0002-5200-6928

Nelli Weiß – *Physical Chemistry, TU Dresden, 01069 Dresden, Germany*

Houman Bahmani Jalali – *Photonic Nanomaterials, Istituto Italiano di Tecnologia, 16163 Genova, Italy; Nanochemistry, Istituto Italiano di Tecnologia, 16163 Genova, Italy;* orcid.org/0000-0001-7212-9098

Francesco di Stasio – *Photonic Nanomaterials, Istituto Italiano di Tecnologia, 16163 Genova, Italy;* orcid.org/0000-0002-2079-3322

Christine Steinbach – *Leibniz-Institut für Polymerforschung Dresden e.V., 01069 Dresden, Germany*

Nikolai Gaponik – *Physical Chemistry, TU Dresden, 01069 Dresden, Germany;* orcid.org/0000-0002-8827-2881

Complete contact information is available at: https://pubs.acs.org/10.1021/acs.chemmater.3c00538

Notes

The authors declare no competing financial interest.

ACKNOWLEDGMENTS

The authors are grateful to S. Goldberg (TU Dresden) for bright-field TEM imaging. A.B. thanks the Graduate Academy of TU Dresden for providing the 'Scholarship for the promotion of early career female scientists of TU Dresden'. The use of the HZDR Ion Beam Center TEM facilities and the funding of TEM Talos by the German Federal Ministry of Education and Research (BMBF; Grant No. 03SF0451) in the framework of HEMCP are acknowledged. F.D.S. and H.B.J. acknowledge support by the European Union's Horizon 2020 research and innovation programme under the Marie Skłodowska-Curie Grant Agreement No. 101024823 (INFLED). This work was supported by the German Research Foundation (DFG) under the project LE 3877/1-1.

REFERENCES

(1) Talapin, D. V.; Lee, J.-S.; Kovalenko, M. V.; Shevchenko, E. V. Prospects of Colloidal Nanocrystals for Electronic and Optoelectronic Applications. *Chem. Rev.* **2010**, *110*, 389–458.

(2) Tang, J.; Kemp, K. W.; Hoogland, S.; Jeong, K. S.; Liu, H.; Levina, L.; Furukawa, M.; Wang, X.; Debnath, R.; Cha, D.; Chou, K. W.; Fischer, A.; Amassian, A.; Asbury, J. B.; Sargent, E. H. Colloidal-Quantum-Dot Photovoltaics Using Atomic-Ligand Passivation. *Nat. Mater.* **2011**, *10*, 765–771.

(3) Song, J. H.; Jeong, S. Colloidal Quantum Dot Based Solar Cells: From Materials to Devices. *Nano Convergence* **2017**, *4*, No. 21.

(4) Li, L.; Daou, T. J.; Texier, I.; Chi, T. T. K.; Liem, N. Q.; Reiss, P. Highly Luminescent $CuInS_2$/ZnS Core/Shell Nanocrystals: Cadmium-Free Quantum Dots for In Vivo Imaging. *Chem. Mater.* **2009**, *21*, 2422–2429.

(5) Jalali, H. B.; De Trizio, L.; Manna, L.; Di Stasio, F. Indium Arsenide Quantum Dots: An Alternative to Lead-Based Infrared Emitting Nanomaterials. *Chem. Soc. Rev.* **2022**, *51*, 9861−9881.
(6) Aldakov, D.; Aurélie, L.; Peter, R. Ternary and Quaternary Metal Chalcogenide Nanocrystals: Synthesis, Properties and Applications. *J. Mater. Chem. C* **2013**, *1*, 3756−3776.
(7) Zhong, H.; Bai, Z.; Zou, B. Tuning the Luminescence Properties of Colloidal I-III-VI Semiconductor Nanocrystals for Optoelectronics and Biotechnology Applications. *J. Phys. Chem. Lett.* **2012**, *3*, 3167−3175.
(8) Sapsford, K. E.; Algar, W. R.; Berti, L.; Gemmill, K. B.; Casey, B. J.; Oh, E.; Stewart, M. H.; Medintz, I. L. Functionalizing Nanoparticles with Biological Molecules: Developing Chemistries that Facilitate Nanotechnology. *Chem. Rev.* **2013**, *113*, 1904−2074.
(9) Yarema, O.; Bozyigit, D.; Rousseau, I.; Nowack, L.; Yarema, M.; Heiss, W.; Wood, V. Highly Luminescent, Size- and Shape-Tunable Copper Indium Selenide Based Colloidal Nanocrystals. *Chem. Mater.* **2013**, *25*, 3753−3757.
(10) Zhong, H.; Wang, Z.; Bovero, E.; Lu, Z.; van Veggel, F. C. J. M.; Scholes, G. D. Colloidal $CuInSe_2$ Nanocrystals in the Quantum Confinement Regime: Synthesis, Optical Properties, and Electroluminescence. *J. Phys. Chem. C* **2011**, *115*, 12396−12402.
(11) Du, J.; Du, Z.; Hu, J. S.; Pan, Z.; Shen, Q.; Sun, J.; Long, D.; Dong, H.; Sun, L.; Zhong, X.; Wan, L. J. Zn-Cu-In-Se Quantum Dot Solar Cells with a Certified Power Conversion Efficiency of 11.6%. *J. Am. Chem. Soc.* **2016**, *138*, 4201−4209.
(12) Zhang, H.; Fang, W.; Wang, W.; Qian, N.; Ji, X. Highly Efficient Zn-Cu-In-Se Quantum Dot-Sensitized Solar Cells through Surface Capping with Ascorbic Acid. *ACS Appl. Mater. Interfaces* **2019**, *11*, 6927−6936.
(13) Stolle, C. J.; Harvey, T. B.; Pernik, D. R.; Hibbert, J. I.; Du, J.; Rhee, D. J.; Akhavan, V. A.; Schaller, R. D.; Korgel, B. A. Multiexciton Solar Cells of $CuInSe_2$ Nanocrystals. *J. Phys. Chem. Lett.* **2014**, *5*, 304−309.
(14) Stolle, C. J.; Schaller, R. D.; Korgel, B. A. Efficient Carrier Multiplication in Colloidal $CuInSe_2$ Nanocrystals. *J. Phys. Chem. Lett.* **2014**, *5*, 3169−3174.
(15) Zhou, Y.; Benetti, D.; Fan, Z.; Zhao, H.; Ma, D.; Govorov, A. O.; Vomiero, A.; Rosei, F. Near Infrared, Highly Efficient Luminescent Solar Concentrators. *Adv. Energy Mater.* **2016**, *6*, No. 1501913.
(16) Li, H.; Wu, K.; Lim, J.; Song, H. J.; Klimov, V. I. Doctor-Blade Deposition of Quantum Dots onto Standard Window Glass for Low-Loss Large-Area Luminescent Solar Concentrators. *Nat. Energy* **2016**, *1*, No. 16157.
(17) Wu, K.; Li, H.; Klimov, V. I. Tandem Luminescent Solar Concentrators Based on Engineered Quantum Dots. *Nat. Photonics* **2018**, *12*, 105−110.
(18) Meinardi, F.; McDaniel, H.; Carulli, F.; Colombo, A.; Velizhanin, K. A.; Makarov, N. S.; Simonutti, R.; Klimov, V. I.; Brovelli, S. Highly Efficient Large-Area Colourless Luminescent Solar Concentrators Using Heavy-Metal-Free Colloidal Quantum Dots. *Nat. Nanotechnol.* **2015**, *10*, 878−885.
(19) Witt, E.; Kolny-Olesiak, J. Recent Developments in Colloidal Synthesis of $CuInSe_2$ Nanoparticles. *Chem. - Eur. J.* **2013**, *19*, 9746−9753.
(20) Allen, P. M.; Bawendi, M. G. Ternary I-III-VI Quantum Dots Luminescent in the Red to Near-Infrared. *J. Am. Chem. Soc.* **2008**, *130*, 9240−9241.
(21) Nose, K.; Omata, T. Shinya Otsuka-Yao-Matsuo, S., Colloidal Synthesis of Ternary Copper Indium Diselenide Quantum Dots and Their Optical Properties. *J. Phys. Chem. C* **2009**, *113*, 3455−3460.
(22) McDaniel, H.; Koposov, A. Y.; Draguta, S.; Makarov, N. S.; Pietryga, J. M.; Klimov, V. I. Simple yet Versatile Synthesis of $CuInSe_xS_{2-x}$ Quantum Dots for Sunlight Harvesting. *J. Phys. Chem. C* **2014**, *118*, 16987−16994.
(23) Rivest, J. B.; Jain, P. K. Cation Exchange on the Nanoscale: An emerging Technique for New Material Synthesis, Device Fabrication, and Chemical Sensing. *Chem. Soc. Rev.* **2013**, *42*, 89−96.
(24) Pearson, R. G. Absolute Electronegativity and Hardness: Application to Inorganic Chemistry. *Inorg. Chem.* **1988**, *27*, 734−740.
(25) Parr, R. G.; Pearson, R. G. Absolute Hardness: Companion Parameter to Absolute Electronegativity. *J. Am. Chem. Soc.* **1983**, *105*, 7512−7516.
(26) Pearson, R. G. Hard and Soft Acids and Bases. *J. Am. Chem. Soc.* **1963**, *85*, 3533−3539.
(27) Beberwyck, B. J.; Surendranath, Y.; Alivisatos, A. P. Cation Exchange: A Versatile Tool for Nanomaterials Synthesis. *J. Phys. Chem. C* **2013**, *117*, 19759−19770.
(28) Gupta, S.; Kershaw, S. V.; Rogach, A. L. 25th Anniversary Article: Ion Exchange in Colloidal Nanocrystals. *Adv. Mater.* **2013**, *25*, 6923−6943.
(29) van der Stam, W.; Bladt, E.; Rabouw, F. T.; Bals, S.; de Mello Donega, C. Near-Infrared Emitting $CuInSe_2/CuInS_2$ Dot Core/Rod Shell Heteronanorods by Sequential Cation Exchange. *ACS Nano* **2015**, *9*, 11430−11438.
(30) Lesnyak, V.; George, C.; Genovese, A.; Prato, M.; Casu, A.; Ayyappan, S.; Scarpellini, A.; Manna, L. Alloyed Copper Chalcogenide Nanoplatelets via Partial Cation Exchange Reactions. *ACS Nano* **2014**, *8*, 8407−8418.
(31) Liu, Y.; Yin, D.; Swihart, M. T. Valence Selectivity of Cation Incorporation into Covellite CuS Nanoplatelets. *Chem. Mater.* **2018**, *30*, 1399−1407.
(32) Lesnyak, V. Chemical Transformations of Colloidal Semiconductor Nanocrystals Advance Their Applications. *J. Phys. Chem. Lett.* **2021**, *12*, 12310−12322.
(33) Lox, J. F. L.; Dang, Z.; Dzhagan, V. M.; Spittel, D.; Martín-García, B.; Moreels, I.; Zahn, D. R. T.; Lesnyak, V. Near-Infrared Cu−In−Se-Based Colloidal Nanocrystals via Cation Exchange. *Chem. Mater.* **2018**, *30*, 2607−2617.
(34) Liu, Y.; Liu, M.; Yin, D.; Qiao, L.; Fu, Z.; Swihart, M. T. Selective Cation Incorporation into Copper Sulfide Based Nanoheterostructures. *ACS Nano* **2018**, *12*, 7803−7811.
(35) De Trizio, L.; Manna, L. Forging Colloidal Nanostructures via Cation Exchange Reactions. *Chem. Rev.* **2016**, *116*, 10852−10887.
(36) Shamraienko, V.; Spittel, D.; Hübner, R.; Samadi Khoshkhoo, M.; Weiß, N.; Georgi, M.; Borchert, K. B. L.; Schwarz, D.; Lesnyak, V.; Eychmüller, A. Cation Exchange on Colloidal Copper Selenide Nanosheets: A Route to Two-Dimensional Metal Selenide Nanomaterials. *J. Mater. Chem. C* **2021**, *9*, 16523−16535.
(37) Lide, D. R. *CRC Handbook of Chemistry and Physics*, 84th ed.; CRC Press: Boca Raton, 2003−2004.
(38) Akkerman, Q. A.; Genovese, A.; George, C.; Prato, M.; Moreels, I.; Cabot, A.; Marras, S.; Curcio, A.; Scarpellini, A.; Pellegrino, T.; Manna, L.; Lesnyak, V. From Binary Cu_2S toTernary Cu-In-S and Quaternary Cu-In-Zn-S Nanocrystals with Tunable Composition via Partial Cation Exchange. *ACS Nano* **2015**, *9*, 521−531.
(39) Lesnyak, V.; Brescia, R.; Messina, G. C.; Manna, L. Cu Vacancies Boost Cation Exchange Reactions in Copper Selenide Nanocrystals. *J. Am. Chem. Soc.* **2015**, *137*, 9315−9323.
(40) Rice, W. D.; McDaniel, H.; Klimov, V. I.; Crooker, S. A. Magneto-Optical Properties of $CuInS_2$ Nanocrystals. *J. Phys. Chem. Lett.* **2014**, *5*, 4105−4109.
(41) Berends, A. C.; Rabouw, F. T.; Spoor, F. C.; Bladt, E.; Grozema, F. C.; Houtepen, A. J.; Siebbeles, L. D.; de Mello Donega, C. Radiative and Nonradiative Recombination in $CuInS_2$ Nanocrystals and $CuInS_2$-Based Core/Shell Nanocrystals. *J. Phys. Chem. Lett.* **2016**, *7*, 3503−3509.
(42) Pinchetti, V.; Lorenzon, M.; McDaniel, H.; Lorenzi, R.; Meinardi, F.; Klimov, V. I.; Brovelli, S. Spectro-Electrochemical Probing of Intrinsic and Extrinsic Processes in Exciton Recombination in I-III-VI_2 Nanocrystals. *Nano Lett.* **2017**, *17*, 4508−4517.
(43) Knowles, K. E.; Nelson, H. D.; Kilburn, T. B.; Gamelin, D. R. Singlet-Triplet Splittings in the Luminescent Excited States of Colloidal Cu^+:CdSe, Cu^+:InP, and $CuInS_2$ Nanocrystals: Charge-Transfer Configurations and Self-Trapped Excitons. *J. Am. Chem. Soc.* **2015**, *137*, 13138−13147.

https://doi.org/10.1021/acs.chemmater.3c00538
Chem. Mater. XXXX, XXX, XXX−XXX

(44) Brovelli, S.; Galland, C.; Viswanatha, R.; Klimov, V. I. Tuning Radiative Recombination in Cu-Doped Nanocrystals via Electrochemical Control of Surface Trapping. *Nano Lett.* **2012**, *12*, 4372−4379.
(45) Fuhr, A. S.; Yun, H. J.; Makarov, N. S.; Li, H.; McDaniel, H.; Klimov, V. I. Light Emission Mechanisms in $CuInS_2$ Quantum Dots Evaluated by Spectral Electrochemistry. *ACS Photonics* **2017**, *4*, 2425−2435.
(46) Li, L.; Pandey, A.; Werder, D. J.; Khanal, B. P.; Pietryga, J. M.; Klimov, V. I. Efficient Synthesis of Highly Luminescent Copper Indium Sulfide-Based Core/Shell Nanocrystals with Surprisingly Long-Lived Emission. *J. Am. Chem. Soc.* **2011**, *133*, 1176−1179.
(47) Chen, Z.; Xie, C.; Yang, F.; Feng, L.; Liang, X.; Xiang, W. Controllable Synthesis of Colloidal $CuInS_2$ Nanocrystals with Tunable Structures and Its Nonlinear Optical Properties. *J. Alloys Compd.* **2014**, *594*, 107−113.
(48) Jara, D. H.; Stamplecoskie, K. G.; Kamat, P. V. Two Distinct Transitions in Cu_xInS_2 Quantum Dots. Bandgap versus Sub-Bandgap Excitations in Copper-Deficient Structures. *J. Phys. Chem. Lett.* **2016**, *7*, 1452−1459.
(49) Knowles, K. E.; Hartstein, K. H.; Kilburn, T. B.; Marchioro, A.; Nelson, H. D.; Whitham, P. J.; Gamelin, D. R. Luminescent Colloidal Semiconductor Nanocrystals Containing Copper: Synthesis, Photophysics, and Applications. *Chem. Rev.* **2016**, *116*, 10820−10851.
(50) Whitham, P. J.; Marchioro, A.; Knowles, K. E.; Kilburn, T. B.; Reid, P. J.; Gamelin, D. R. Single-Particle Photoluminescence Spectra, Blinking, and Delayed Luminescence of Colloidal $CuInS_2$ Nanocrystals. *J. Phys. Chem. C* **2016**, *120*, 17136−17142.
(51) Zang, H.; Li, H.; Makarov, N. S.; Velizhanin, K. A.; Wu, K.; Park, Y. S.; Klimov, V. I. Thick-Shell $CuInS_2$/ZnS Quantum Dots with Suppressed "Blinking" and Narrow Single-Particle Emission Line Widths. *Nano Lett.* **2017**, *17*, 1787−1795.
(52) Bora, A.; Prudnikau, A.; Fu, N.; Hübner, R.; Borchert, K. B. L.; Schwarz, D.; Gaponik, N.; Lesnyak, V. Seed-Mediated Synthesis of Photoluminescent Cu−Zn−In−S Nanoplatelets. *Chem. Mater.* **2022**, *34*, 9251−9260.
(53) Koo, B.; Patel, R. N.; Korgel, B. A. Synthesis of $CuInSe_2$ Nanocrystals with Trigonal Pyramidal Shape. *J. Am. Chem. Soc.* **2009**, *131*, 3134−3135.
(54) Tang, J.; Hinds, S.; Kelley, S. O.; Sargent, E. H. Synthesis of Colloidal $CuGaSe_2$, $CuInSe_2$, and $Cu(InGa)Se_2$ Nanoparticles. *Chem. Mater.* **2008**, *20*, 6906−6910.
(55) Norako, M. E.; Brutchey, R. L. Synthesis of Metastable Wurtzite $CuInSe_2$ Nanocrystals. *Chem. Mater.* **2010**, *22*, 1613−1615.
(56) Cassette, E.; Pons, T.; Bouet, C.; Helle, M.; Bezdetnaya, L.; Marchal, F.; Dubertret, B. Synthesis and Characterization of Near-Infrared Cu−In−Se/ZnS Core/Shell Quantum Dots for In vivo Imaging. *Chem. Mater.* **2010**, *22*, 6117−6124.
(57) Llorente, V. B.; Dzhagan, V. M.; Gaponik, N.; Iglesias, R. A.; Zahn, D. R. T.; Lesnyak, V. Electrochemical Tuning of Localized Surface Plasmon Resonance in Copper Chalcogenide Nanocrystals. *J. Phys. Chem. C* **2017**, *121*, 18244−18253.
(58) Khoshkhoo, M. S.; Lox, J. F. L.; Koitzsch, A.; Lesny, H.; Joseph, Y.; Lesnyak, V.; Eychmüller, A. Highly Conductive Copper Selenide Nanocrystal Thin Films for Advanced Electronics. *ACS Appl. Electron. Mater.* **2019**, *1*, 1560−1569.
(59) Wolf, A.; Kodanek, T.; Dorfs, D. Tuning the LSPR in Copper Chalcogenide Nanoparticles by Cation Intercalation, Cation Exchange and Metal Growth. *Nanoscale* **2015**, *7*, 19519−19527.
(60) Dorfs, D.; Hartling, T.; Miszta, K.; Bigall, N. C.; Kim, M. R.; Genovese, A.; Falqui, A.; Povia, M.; Manna, L. Reversible Tunability of the Near-Infrared Valence Band Plasmon Resonance in $Cu_{2-x}Se$ Nanocrystals. *J. Am. Chem. Soc.* **2011**, *133*, 11175−11180.
(61) van der Stam, W.; Berends, A. C.; Rabouw, F. T.; Willhammar, T.; Ke, X.; Meeldijk, J. D.; Bals, S.; de Mello Donega, C. Luminescent $CuInS_2$ Quantum Dots by Partial Cation Exchange in $Cu_{2-x}S$ Nanocrystals. *Chem. Mater.* **2015**, *27*, 621−628.
(62) Yarema, O.; Yarema, M.; Wood, V. Tuning the Composition of Multicomponent Semiconductor Nanocrystals: The Case of I−III−VI Materials. *Chem. Mater.* **2018**, *30*, 1446−1461.
(63) Pan, D.; An, L.; Sun, Z.; Hou, W.; Yang, Y.; Yang, Z.; Lu, Y. Synthesis of Cu-In-S Ternary Nanocrystals with Tunable Structure and Composition. *J. Am. Chem. Soc.* **2008**, *130*, 5620−5621.
(64) Zhao, Y.; Pan, H.; Lou, Y.; Qiu, X.; Zhu, J.; Burda, C. Plasmonic $Cu_{2-x}S$ Nanocrystals: Optical and Structural Properties of Copper-Deficient Copper(I) Sulfides. *J. Am. Chem. Soc.* **2009**, *131*, 4253−4261.
(65) De Trizio, L.; Gaspari, R.; Bertoni, G.; Kriegel, I.; Moretti, L.; Scotognella, F.; Maserati, L.; Zhang, Y.; Messina, G. C.; Prato, M.; Marras, S.; Cavalli, A.; Manna, L. $Cu_{3-x}P$ Nanocrystals as a Material Platform for Near-Infrared Plasmonics and Cation Exchange Reactions. *Chem. Mater.* **2015**, *27*, 1120−1128.
(66) Panthani, M. G.; Stolle, C. J.; Reid, D. K.; Rhee, D. J.; Harvey, T. B.; Akhavan, V. A.; Yu, Y.; Korgel, B. A. $CuInSe_2$ Quantum Dot Solar Cells with High Open-Circuit Voltage. *J. Phys. Chem. Lett.* **2013**, *4*, 2030−2034.
(67) McDaniel, H.; Fuke, N.; Pietryga, J. M.; Klimov, V. I. Engineered $CuInSe_xS_{2-x}$ Quantum Dots for Sensitized Solar Cells. *J. Phys. Chem. Lett.* **2013**, *4*, 355−361.
(68) Xie, R.; Rutherford, M.; Peng, X. Formation of High-Quality I-III-VI Semiconductor Nanocrystals by Tuning Relative Reactivity of Cationic Precursors. *J. Am. Chem. Soc.* **2009**, *131*, 5691−5697.
(69) De Trizio, L.; Prato, M.; Genovese, A.; Casu, A.; Povia, M.; Simonutti, R.; Alcocer, M. J. P.; D'Andrea, C.; Tassone, F.; Manna, L. Strongly Fluorescent Quaternary Cu−In−Zn−S Nanocrystals Prepared from $Cu_{1-x}InS_2$ Nanocrystals by Partial Cation Exchange. *Chem. Mater.* **2012**, *24*, 2400−2406.
(70) Hinterding, S. O. M.; Mangnus, M. J. J.; Prins, P. T.; Jobsis, H. J.; Busatto, S.; Vanmaekelbergh, D.; de Mello Donega, C.; Rabouw, F. T. Unusual Spectral Diffusion of Single $CuInS_2$ Quantum Dots Sheds Light on the Mechanism of Radiative Decay. *Nano Lett.* **2021**, *21*, 658−665.
(71) Berends, A. C.; Mangnus, M. J. J.; Xia, C.; Rabouw, F. T.; de Mello Donega, C. Optoelectronic Properties of Ternary I-III-VI_2 Semiconductor Nanocrystals: Bright Prospects with Elusive Origins. *J. Phys. Chem. Lett.* **2019**, *10*, 1600−1616.
(72) Liu, H.; Cai, P.; McHugh, K. J.; Perkinson, C. F.; Li, L.; Wang, S.; Wang, W.; Jiao, M.; Luo, X.; Jing, L. Aqueous Synthesis of Bright Near-Infrared-Emitting Zn-Cu-In-Se Quantum Dots for Multiplexed Detection of Tumor Markers. *Nano Res.* **2022**, *15*, 8351−8359.
(73) Galle, T.; Spittel, D.; Weiss, N.; Shamraienko, V.; Decker, H.; Georgi, M.; Hubner, R.; Metzkow, N.; Steinbach, C.; Schwarz, D.; Lesnyak, V.; Eychmüller, A. Simultaneous Ligand and Cation Exchange of Colloidal CdSe Nanoplatelets toward PbSe Nanoplatelets for Application in Photodetectors. *J. Phys. Chem. Lett.* **2021**, *12*, 5214−5220.
(74) Sonntag, L.; Shamraienko, V.; Fan, X.; Khoshkhoo, M. S.; Kneppe, D.; Koitzsch, A.; Gemming, T.; Hiekel, K.; Leo, K.; Lesnyak, V.; Eychmüller, A. Colloidal PbS Nanoplatelets Synthesized via Cation Exchange for Electronic Applications. *Nanoscale* **2019**, *11*, 19370−19379.
(75) Wang, H.; Butler, D. J.; Straus, D. B.; Oh, N.; Wu, F.; Guo, J.; Xue, K.; Lee, J. D.; Murray, C. B.; Kagan, C. R. Air-Stable $CuInSe_2$ Nanocrystal Transistors and Circuits via Post-Deposition Cation Exchange. *ACS Nano* **2019**, *13*, 2324−2333.
(76) Rosen, E. L.; Buonsanti, R.; Llordes, A.; Sawvel, A. M.; Milliron, D. J.; Helms, B. A. Exceptionally Mild Reactive Stripping of Native Ligands from Nanocrystal Surfaces by Using Meerwein's Salt. *Angew. Chem., Int. Ed.* **2012**, *51*, 684−689.

https://doi.org/10.1021/acs.chemmater.3c00538
Chem. Mater. XXXX, XXX, XXX−XXX